New Applications and Advances of the GPS Radio Occultation Technology as recovered by Analysis of the FORMOSAT-3 and CHAMP Data-Base

A.G.Pavelyev[1], J. Wickert[2], Y.A. Liou[3], V.N. Gubenko[1], A.A. Pavelyev[1]

[1]Institute of Radio Engineering and Electronics of the Russian Academy of Sciences, (IRE RAS), Fryazino, Vvedenskogo sq. 1, 141191 Moscow region, Russia E-mail pvlv@ms.ire.rssi.ru

[2]GeoForschungsZentrum Potsdam, Department Geodesy & Remote Sensing, Telegrafenberg A17, 14473 Potsdam, Germany, E-mail: wickert@gfz-potsdam.de, Phone: +49- 331-288-1168; Fax: +49-331-288-1169

[3]Center for Space and Remote Sensing Research, National Central University, Chung-Li, 320, Taiwan.

E-mail: yueian@csrsr.ncu.edu.tw Fax: +886 3 4254908

September 20 OPAC 3 Graz Austria

Outline

Introduction

1. Advances and refinements in RO technology

-Connection between the phase and amplitude variations and its validation

-Analysis of possibility to locate layered structures and measuring horizontal gradients in the atmosphere and lower ionosphere

2. Internal waves in the neutral atmosphere

Examples of the internal wave-breaking effect in the atmosphere

-Analysis of the dispersion and polarization relationships for gravity waves (GW)

-Portrait of internal waves as obtained from the RO data

-Geographical and seasonal distribution of internal waves

Conclusions

Introduction. Scheme of RO measurements

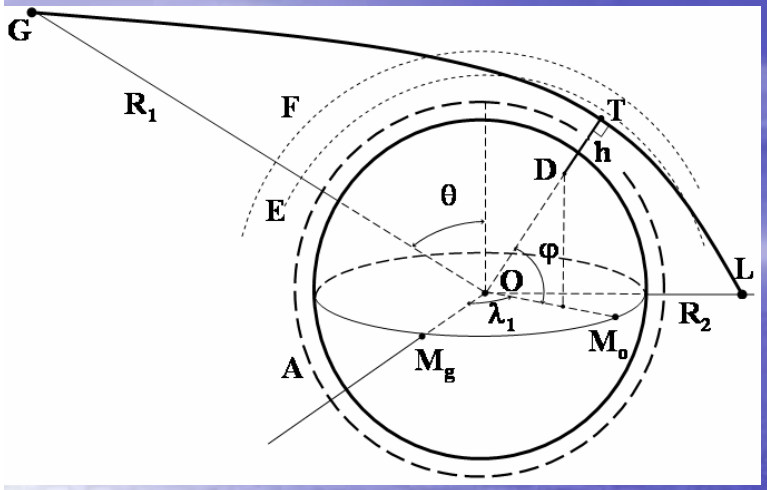

High-precision GPS radio signals at two frequencies F1=1575.42 and F2=1227.6 MHz emitted by the GPS satellite (point G) arrive at the receiver onboard of the LEO satellite (point L) along the ray GTL. The results of registration which are the 1-D radio-holographic images of the propagation medium consist of the phase and amplitude variations at two GPS frequencies. In the case of spherical symmetry these variations are caused mainly owing to the medium influence at the tangent point T which coincides with the ray perigee which corresponds to the center of symmetry – point O. Because location of point O is supposed to be known the geographical coordinates of point T can be evaluated by use of orbital data of GPS and LEO satellites. Analysis of RO data delivers the vertical profile of the refractivity N(h) in the atmosphere. After the usage of the gas state and hydrostatic equilibrium equations one can find the vertical profiles of pressure p(h) and temperature T(h).

Vertical profiles of the refractivity N(h), pressure p(h) and temperature T(h)

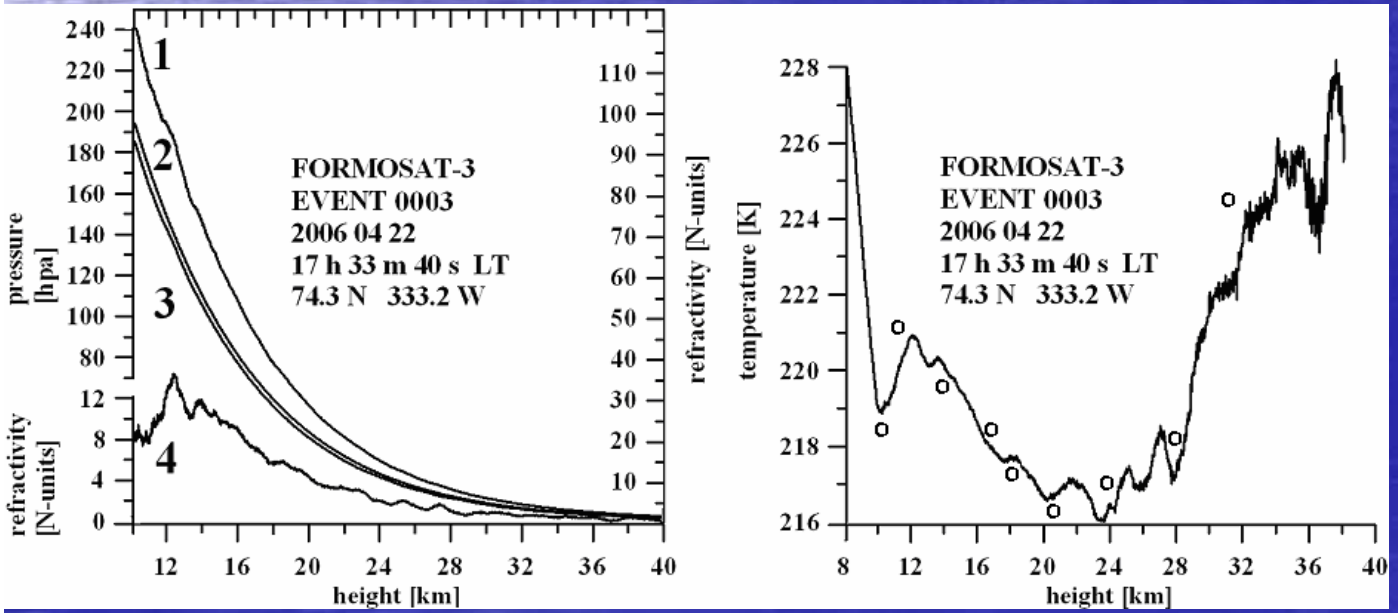

Left panel: Results of retrieving the vertical profiles of refractivity *N(h) [N-units]* and pressure *P(h) [hPa]* from the phase delay *Φ1(t)*. The top left vertical axis corresponds to pressure (curve 1) and the bottom left vertical axis is relevant to the refractivity perturbations (curve 4). The right vertical axis corresponds to the vertical profiles of the refractivity calculated by use of standard atmospheric model (curve 2) and the refractivity retrieved from the RO data (curve 3). Right panel: Results of retrieving the vertical profile of temperature *T(h) [K]*. Open circles indicate the results of NCEP analysis.

The temperature vertical profiles above the equatorial and tropical part of the South America (left and right panel, respectively)

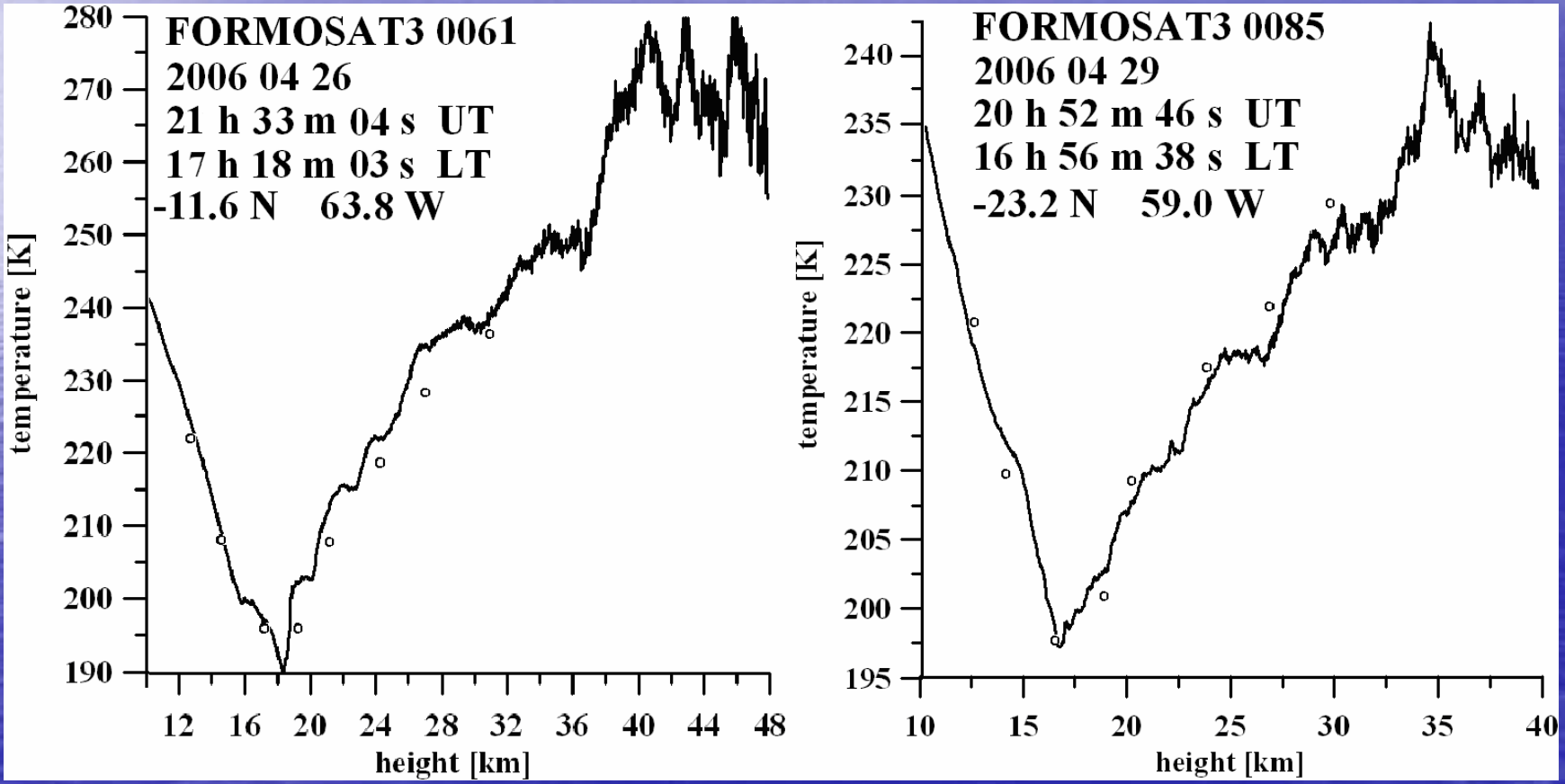

The temperature vertical profiles in the moderate latitudes: the Southern part of the Indian Ocean and the Northern part of the Pacific Ocean (left and right)

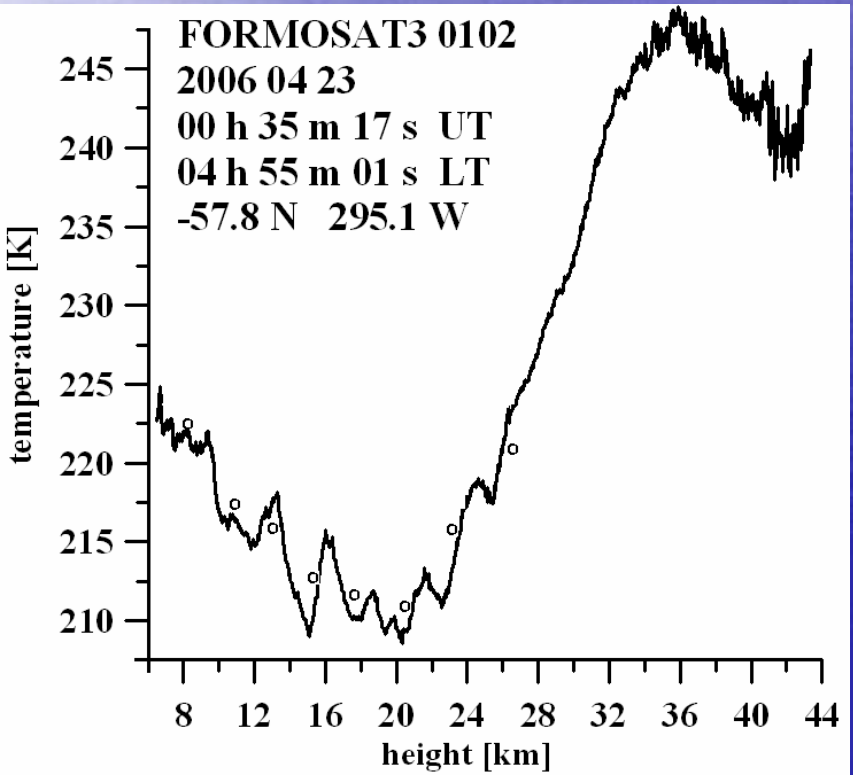

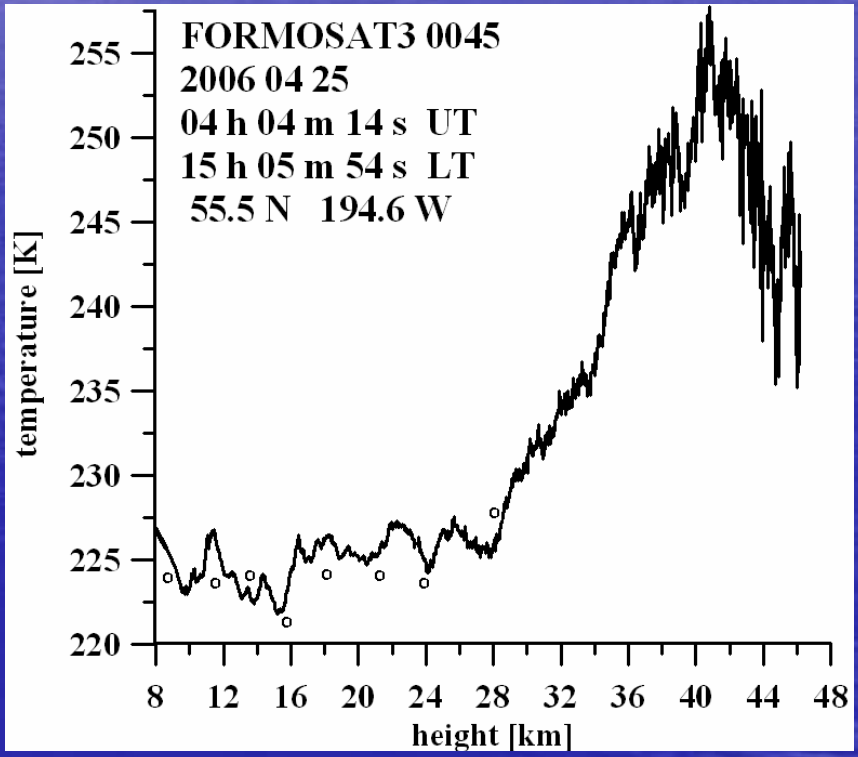

Connection between the amplitude and phase in RO measurements via classical dynamic equation-type (Liou and Pavelyev, GRL, 2006; Pavelyev et al., JGR, 2007)

definition of the phase path excess $\Phi(p)$

$$\Phi(p)=L(p)+\kappa(p)-R_0,\ L(p)=d_1+d_2+p\xi(p),\quad \xi(p)=-d\kappa(p)/dp \quad (1)$$

$\xi(p)$ *is the refraction angle*

definition of the refraction attenuation

$$X(p)=pR_0^2[R_1R_2d_1d_2\sin\theta\,|\partial\theta/\partial p|]^{-1}=A^2/A_0^2, \quad (2)$$

$$\partial\theta/\partial p=d\xi/dp-(1/d_1+1/d_2),\qquad d_{1,2}=(R_{1,2}^2-p^2)^{1/2} \quad (3)$$

$F=ma$, (4) connects the amplitude and phase path excess via classical dynamic equation-type:

$$F=1-X(t),\ a=d^2\Phi(t)/dt^2,\ m=q/(dp_s/dt)^2,$$

$$q=d_1d_2/R_0 \quad (5)$$

Eqs. (4) and (5) allow one to recalculate the phase path excess $\Phi(t)$ to the refraction attenuation X_p. Eq. (5) allows one to estimate the absorption coefficient η from ratio $\eta=X_a/X_p$.

$\Phi(t)=\Phi_u(t)+\Phi_l(t)$, $\Phi(t)$ *is a sum of the upper (slow changing) and lower ionosphere contributions*

$$1-X(t)=m[d^2\Phi_u(t)/dt^2+d^2\Phi_l(t)/dt^2]\approx md^2\Phi_l(t)/dt^2 \quad (6)$$

$$d^2\Phi_l(t)/dt^2\approx-\omega_0^2\Phi_l(t),\ \omega_0^2=4\pi^2v_\perp^2/\lambda_v^2,$$

more simple relations between the phase $\Phi_l(t)$ and intensity scintillations

$$X(t)-1=4\pi^2R_0^{-1}d_1d_2\,\Phi_l(t)/\lambda_v^2 \quad (7)$$

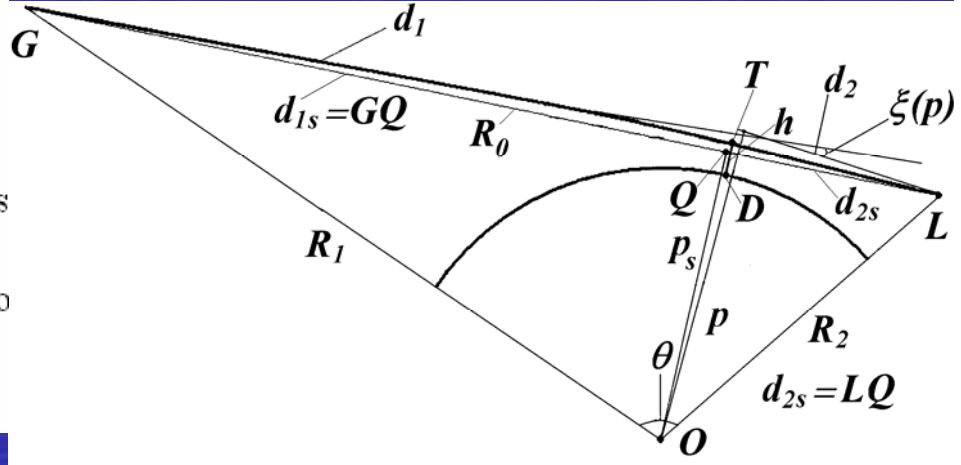

Right: recalculation of the phase variations to the refraction attenuation and comparison with the RO amplitude data (curve 1) (CHAMP data). Curves 2, 3 and 4 correspond to the refraction attenuation retrieved from the phase excess data (left, curves 1-3). Curves 5 are relevant to the standard refraction attenuation vertical profile

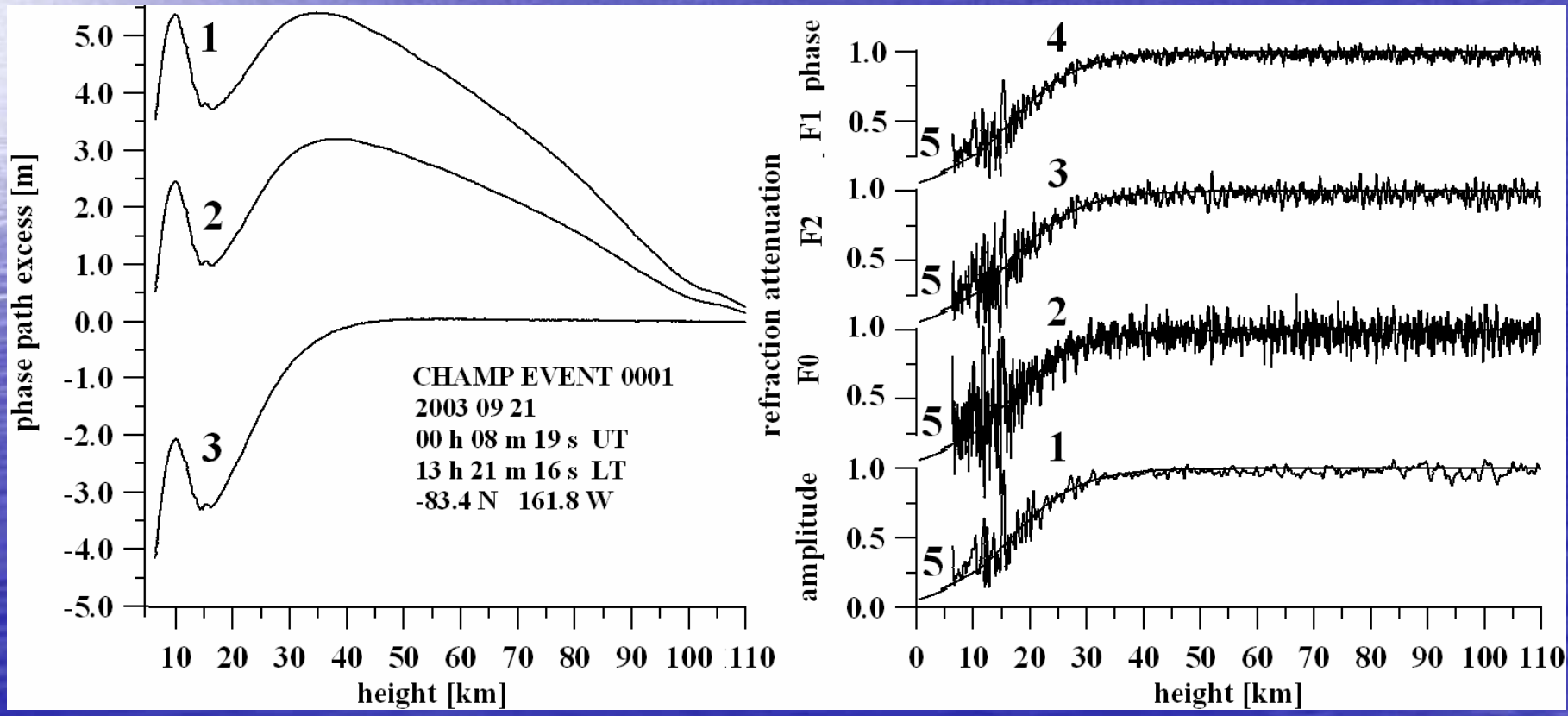

Comparison of the refraction attenuations Xa and Xp retrieved from the FORMOSAT-3 amplitude and phase RO data via equation (4) (neutral atmosphere and lower ionosphere). The antenna's amplitude diagram influence is seen clearly in the intensity data.

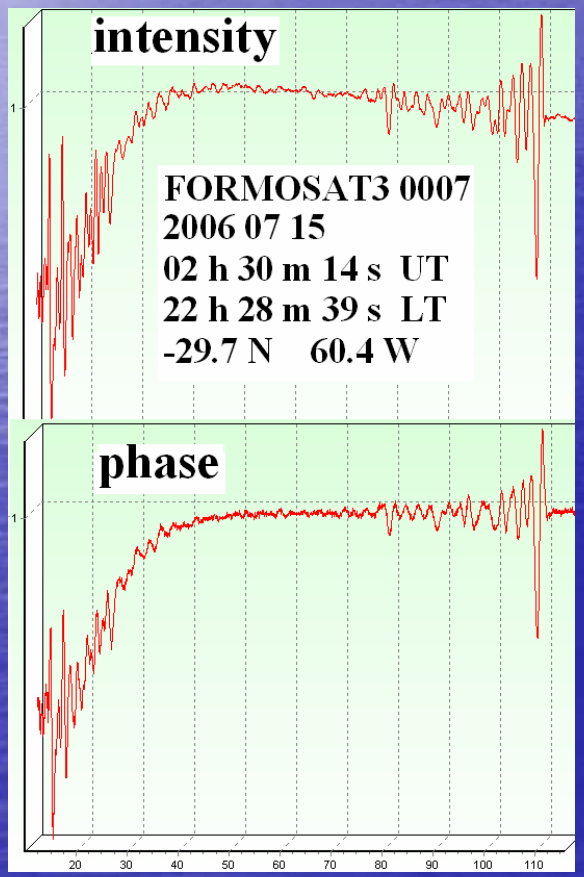

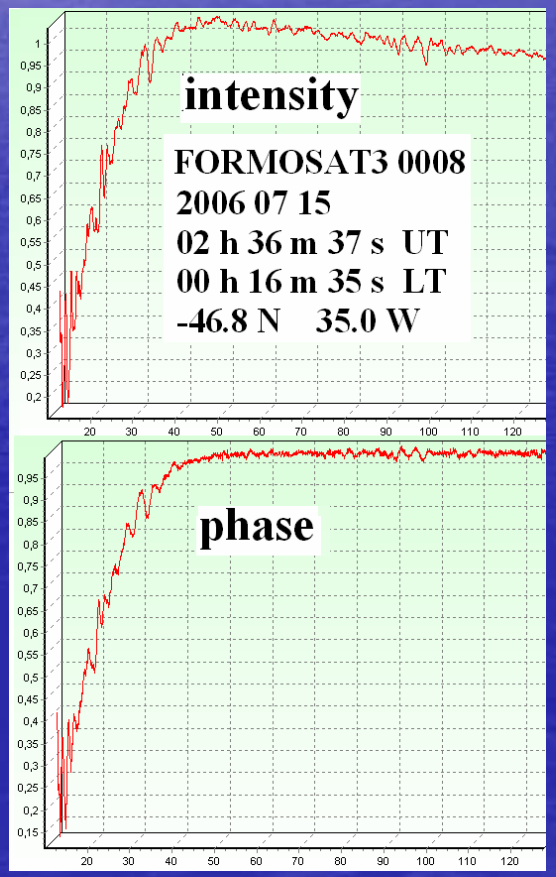

VALIDATION OF CONNECTION (7) BETWEEN THE PHASE PATH EXCESS AND AMPLITUDE VARIATIONS

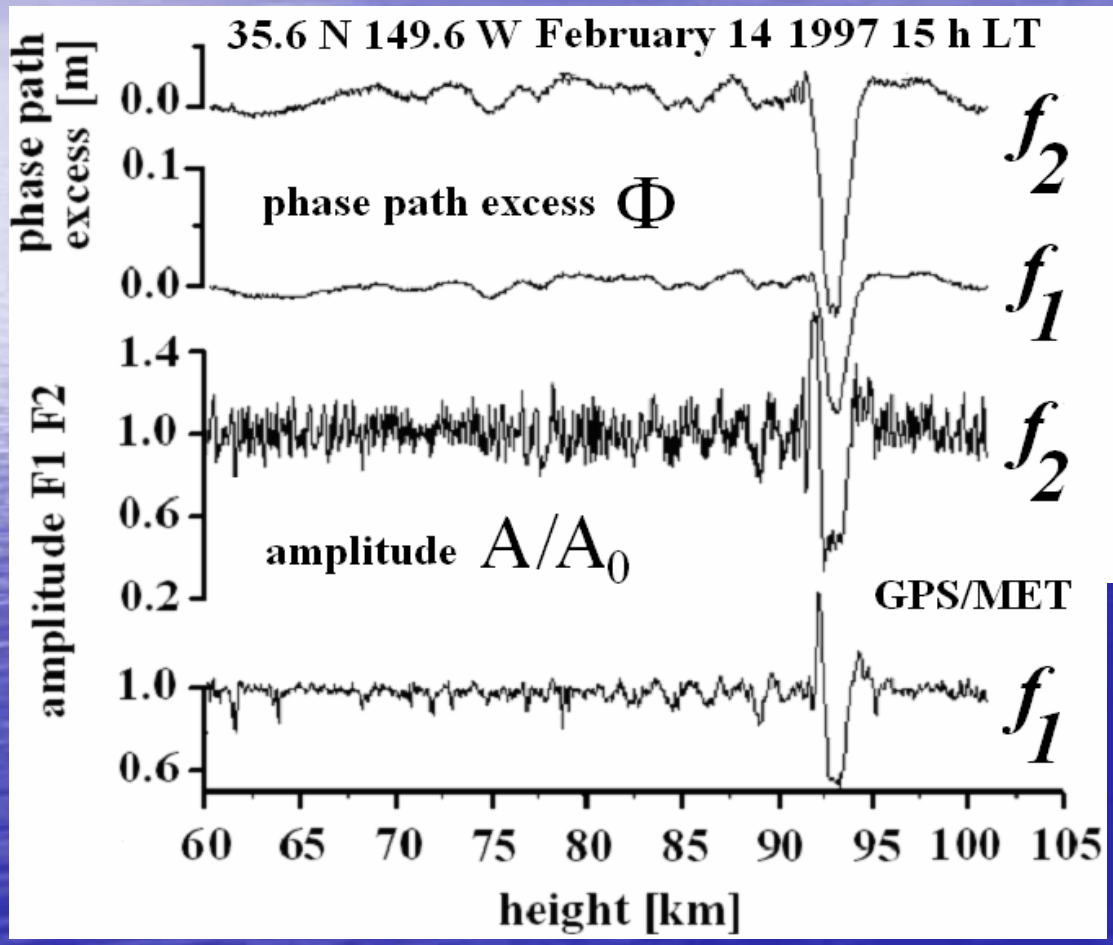

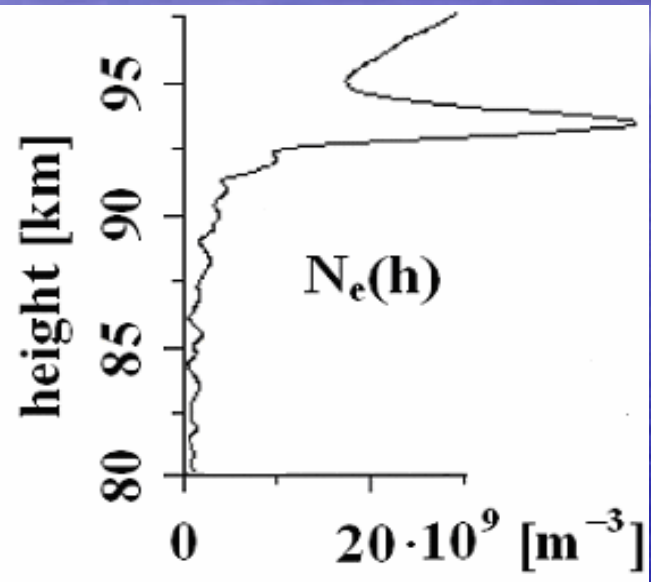

ADVANCED METHOD FOR LOCATION OF LAYERED STRUCTURES IN THE ATMOSPHERE AND IONOSPHERE

$$m=[1-X(t)]/d^2\Phi(t)/dt^2 \quad (8)$$

$$m=d_1d_2R_0^{-1}(dp_s/dt)^{-2} \quad (9)$$

$$m(t_k)=\{\sum_{i=k-M}^{i=k+M}[X(t_i)-1]^2/\sum_{i=k-M}^{i=k+M}[a(t_i)]^2\}^{1/2}, \quad (A)$$

$$m(t_k)=\sum_{i=k-M}^{i=k+M}[X(t_i)-1]a(t_i)/\sum_{i=k-M}^{i=k+M}[a(t_i)]^2, \quad (B)$$

$$dp_s/dt=v+(w-v)d_{1s}/R_0 \quad (10)$$

$$d_{2s}=2mw^2[1+2\beta(v/w-1)+(1-4\beta v/w)^{1/2}]^{-1},$$

$$\beta=mw^2/R_0,\ D=d_{2s}-(R_2^2-p_{s1}^2)^{1/2} \quad (11)$$

where v, w are the velocity components of the GPS and LEO satellites, respectively, which are perpendicular to the straight line GL in the plane GOL.

Previously Sokolovskiy et al., GRL, 2002, and Gorbunov et al., Int.J. Rem. Sens., 2002, applied the radio-holographic back-propagation method to locate the ionospheric irregularities. We propose an alternative method to locate layered structures in the ionosphere and atmosphere Eqs. (8)-(11) can be used to find . the distance LT *d'2s* from simultaneous observation of the phase and intensity variations of radio wave. To achieve this, one can find *m* from (8) as a ratio of the intensity changes to the phase acceleration variations and then the distance *D* can be evaluated from the relationship (11). The horizontal gradient in a layered structure and its height can be estimated by use of displacement *D*. The value *m* can be also estimated by statistical manner from (A) and (B). In this case the different values of *D* can be obtained.

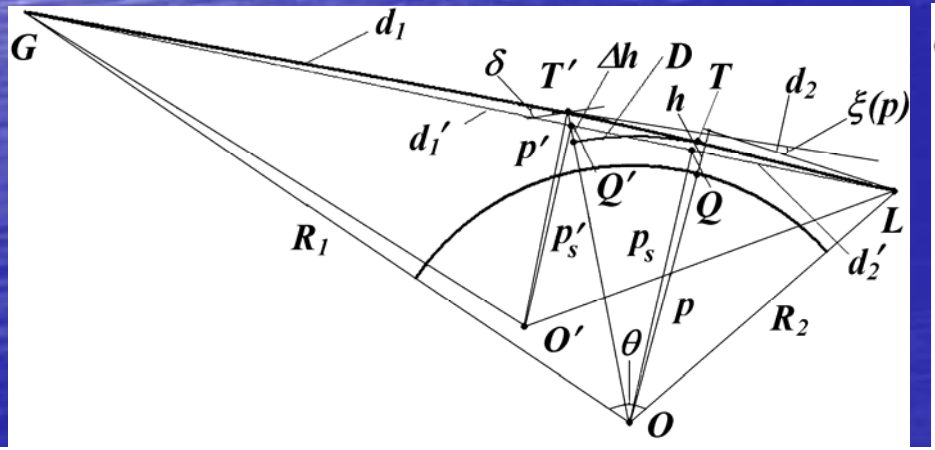

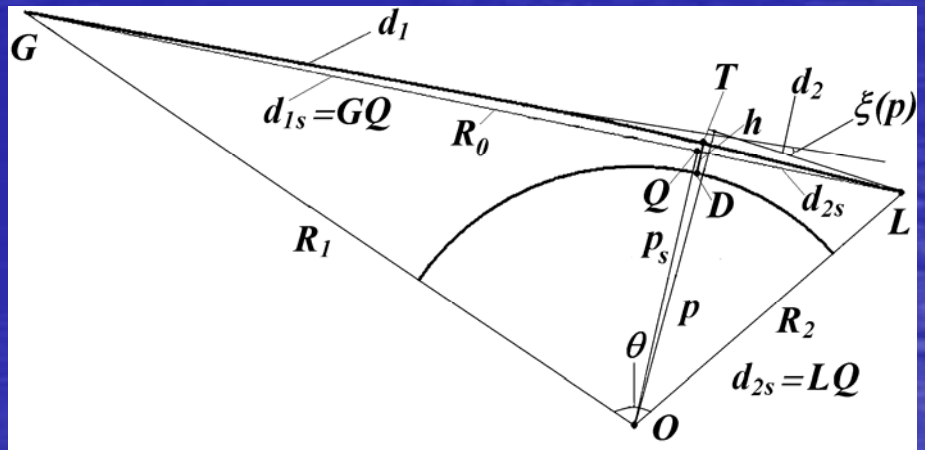

Evidence of atmospheric origin of the phase and amplitude variations in RO signal. Comparison of the refraction attenuations *Xp* and *Xa* calculated from the FORMOSAT-3 phase (curve 1) and amplitude (curve 2) data. Right panel. Displacement *D* of the tangent point *T* calculated by use of equations (A) and (B) (curve 1 and 2, respectively)

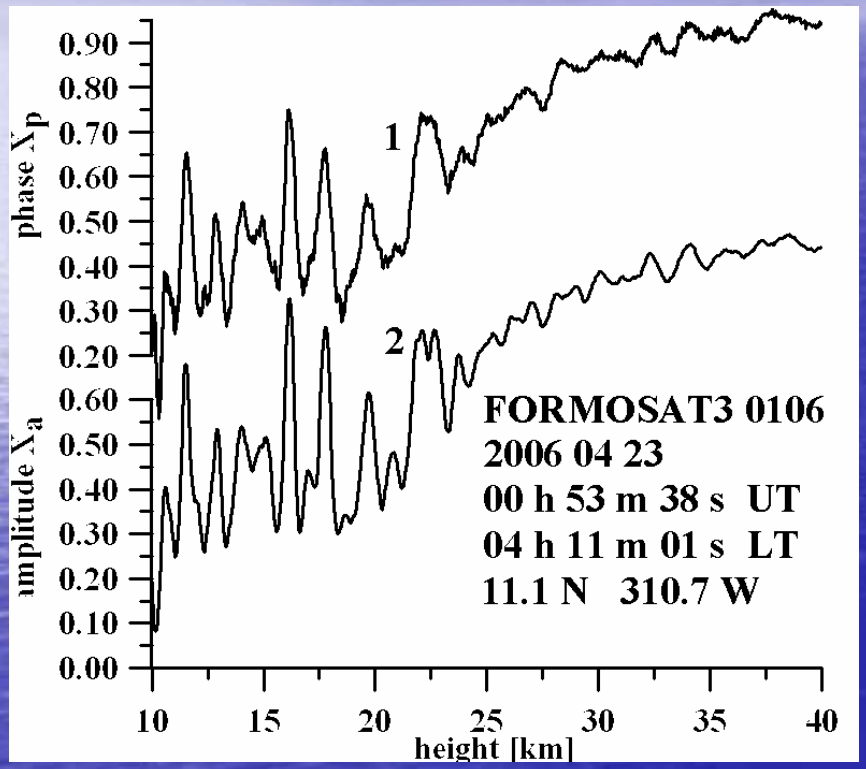

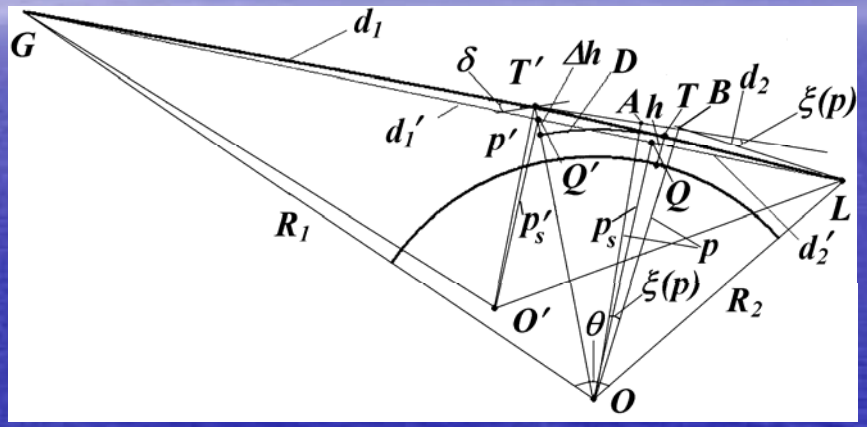

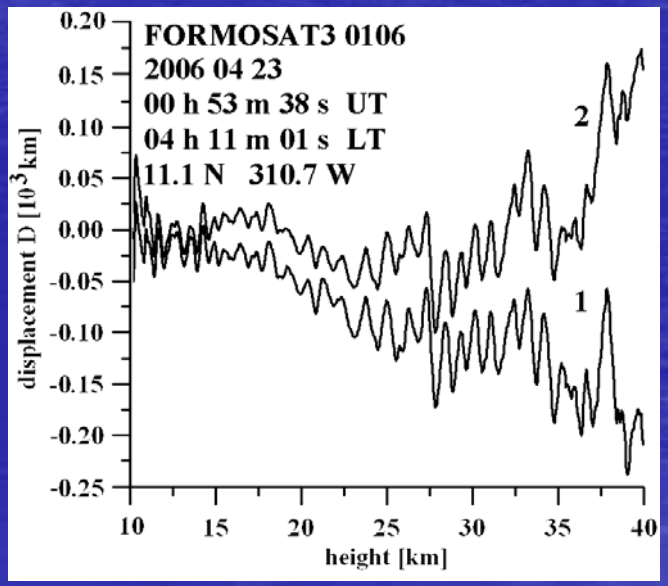

Lower ionosphere. Comparison of the refraction attenuation recalculated from the phase path excess data *Xp*, and refraction attenuation *Xa* found from the amplitude data at the first GPS frequency F1 (curves 1 and 2), results of estimation of distance D (curve 3) (left panel) and retrieved variations of the electron density and its gradients (curves 3 and 4) (right panel).

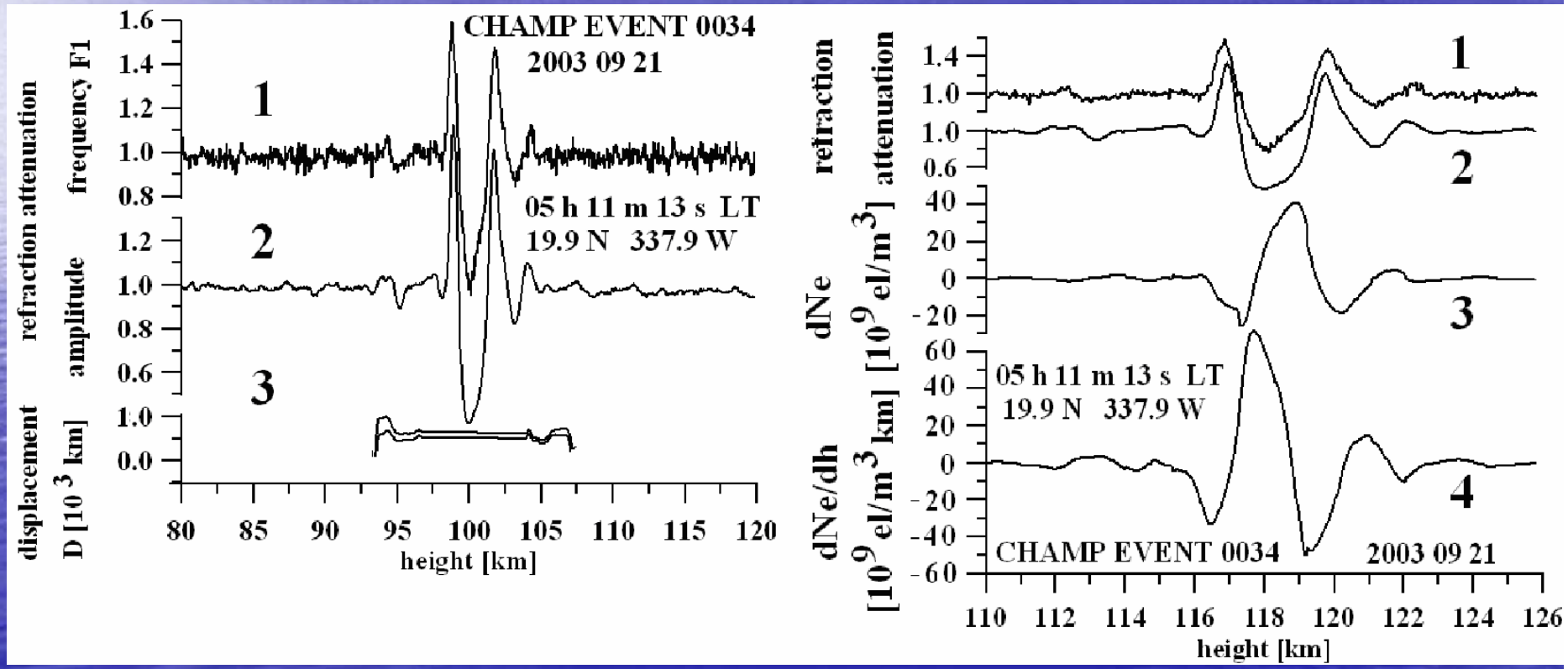

Lower ionosphere. Comparison of the refraction attenuation recalculated from the phase path excess data *Xp*, and refraction attenuation *Xa* found from the amplitude data at the first GPS frequency F1 (curves 1 and 2), results of estimation of distance D and height of the layer h (table 1, right) .

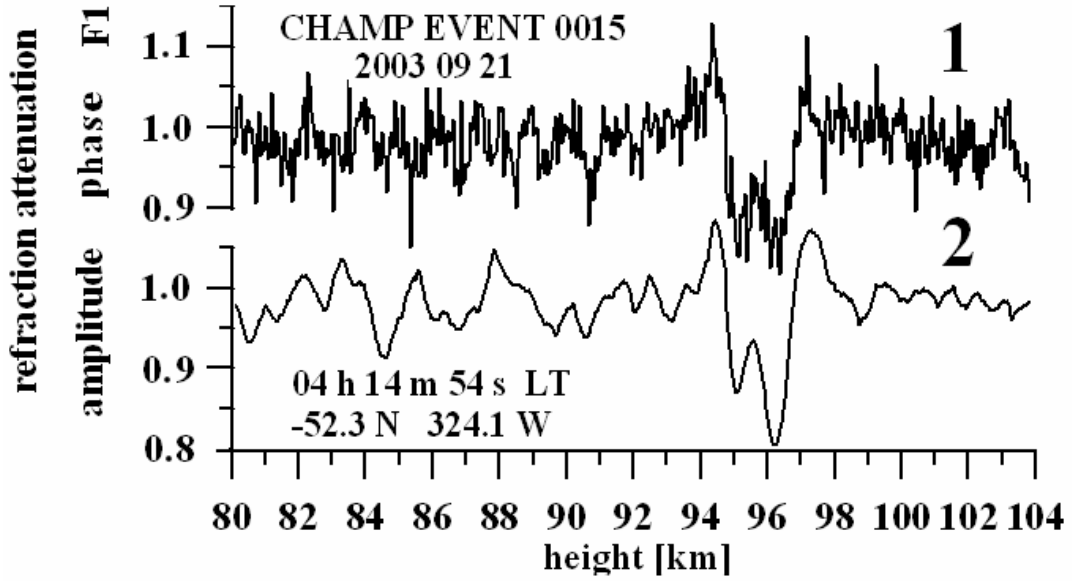

Table 1. Displacement *D* and correction Δh in the height of tangent point

Height *h* [km]	Distance *D* [km]	$\Delta h = d^2/2r$ [km]	Refraction attenuation (F1 phase data) X_p	Refraction attenuation (F1 amplitude data) X_a	Ratio *m* refraction attenuation /phase acceleration variations [s^2/m]
95.746	52.9	.21	.8987	.8956	.3762
95.700	9.3	.00	.9010	.9000	.3685
95.655	-26.5	.05	.9031	.9038	.3621
95.610	61.5	.29	.9096	.9065	.3776
95.564	8.6	.00	.9094	.9086	.3683
95.519	-121.7	1.15	.9051	.9102	.3452
95.474	43.5	.14	.9145	.9122	.3744
95.428	28.9	.06	.9143	.9127	.3718
95.383	-121.5	1.15	.9098	.9146	.3452
95.338	-14.5	.01	.9152	.9154	.3641
95.292	47.0	.17	.9201	.9179	.3749
95.247	-105.4	.86	.9179	.9216	.3480
95.201	-59.2	.27	.9239	.9256	.3561
95.156	64.9	.32	.9323	.9298	.3780
95.111	-179.1	2.50	.9317	.9373	.3349
95.065	-33.8	.08	.9428	.9434	.3605

Gravity waves in RO measurements: background

GWs play a decisive role in affecting the atmospheric circulation and temperature regime [*Friits and Alexander*, 2003]. For theoretical studies it is important to have the experimental data showing the phase and amplitude dependence of the GWs on height. The RO method can be applied to measure the GW parameters on the global scale. Analysis of the temperature variations found from the RO phase data furnishes an opportunity to investigate the global morphology of the GWs activity in the stratosphere and to measure the GWs statistical characteristics in the atmosphere as shown by *Steiner and Kirchengast* [2000], *Tsuda et al.* [2000], and *Tsuda and Hocke* [2002]. The amplitude channels of the RO signal give new potential and capability for the RO research and for the observation of the quasi-regular structures in the atmospheric and ionospheric waves [*Kalashnikov et. al.*, 1986; *Pavelyev et al.*, 2002; Sokolovskii,2000; *Igarashi et al.*, 2000, 2001; *Liou et al.*, 2002, 2003].

Wave structures observed in the amplitude and phase data. Comparison of the refraction attenuations Xa and Xp retrieved from the FORMOSAT-3 amplitude and phase RO data

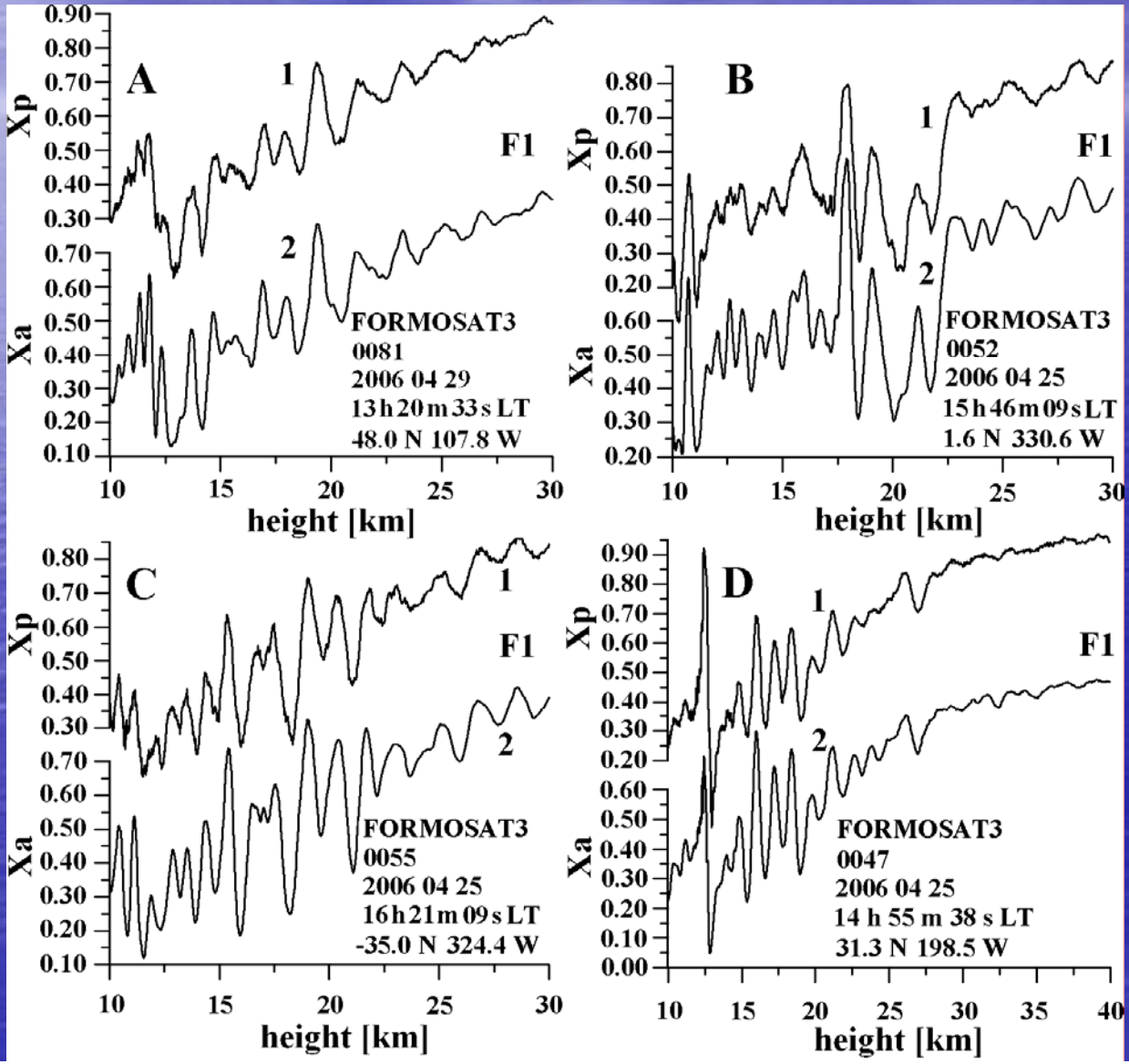

WAVE BREAKING CHAMP RO EVENT

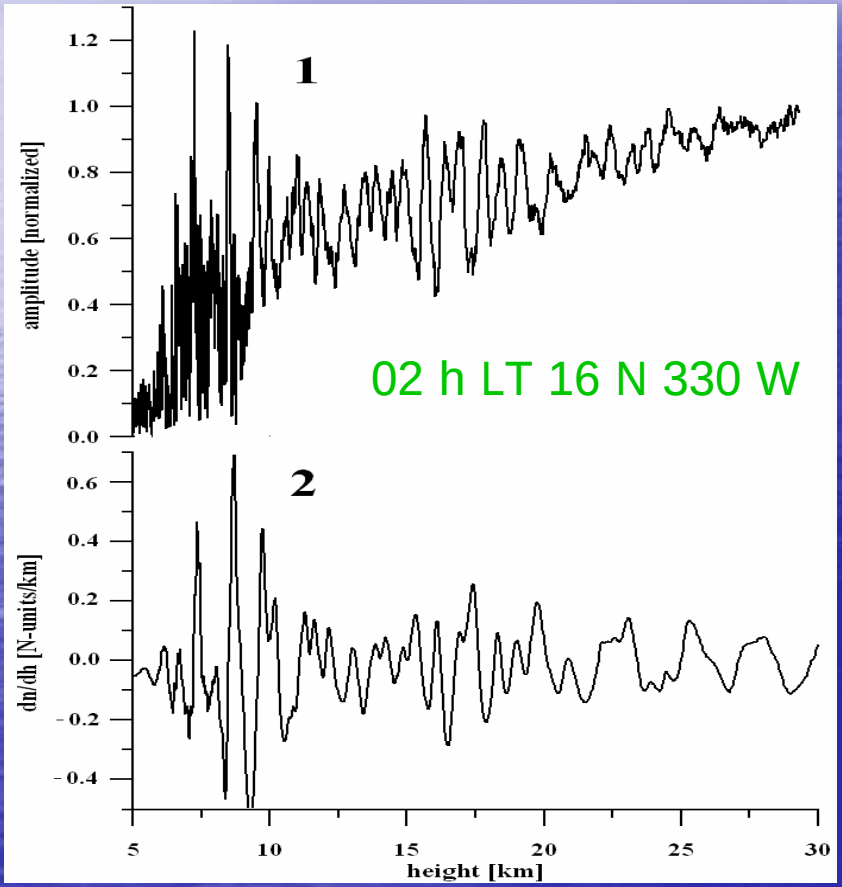

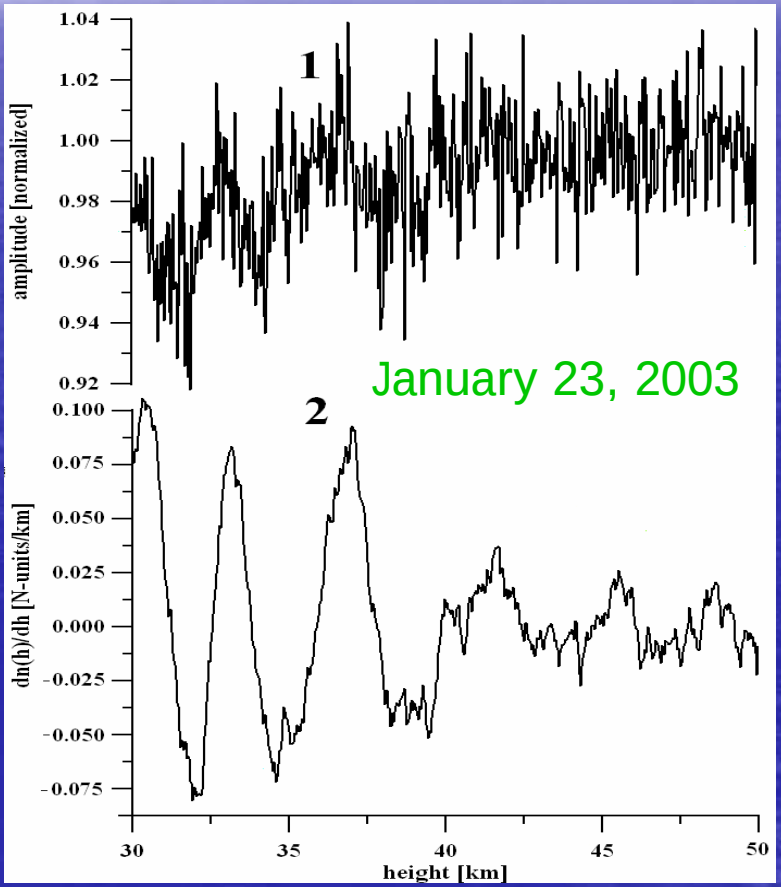

Radio-image of internal waves. Note a breaking effect at 38-43 km

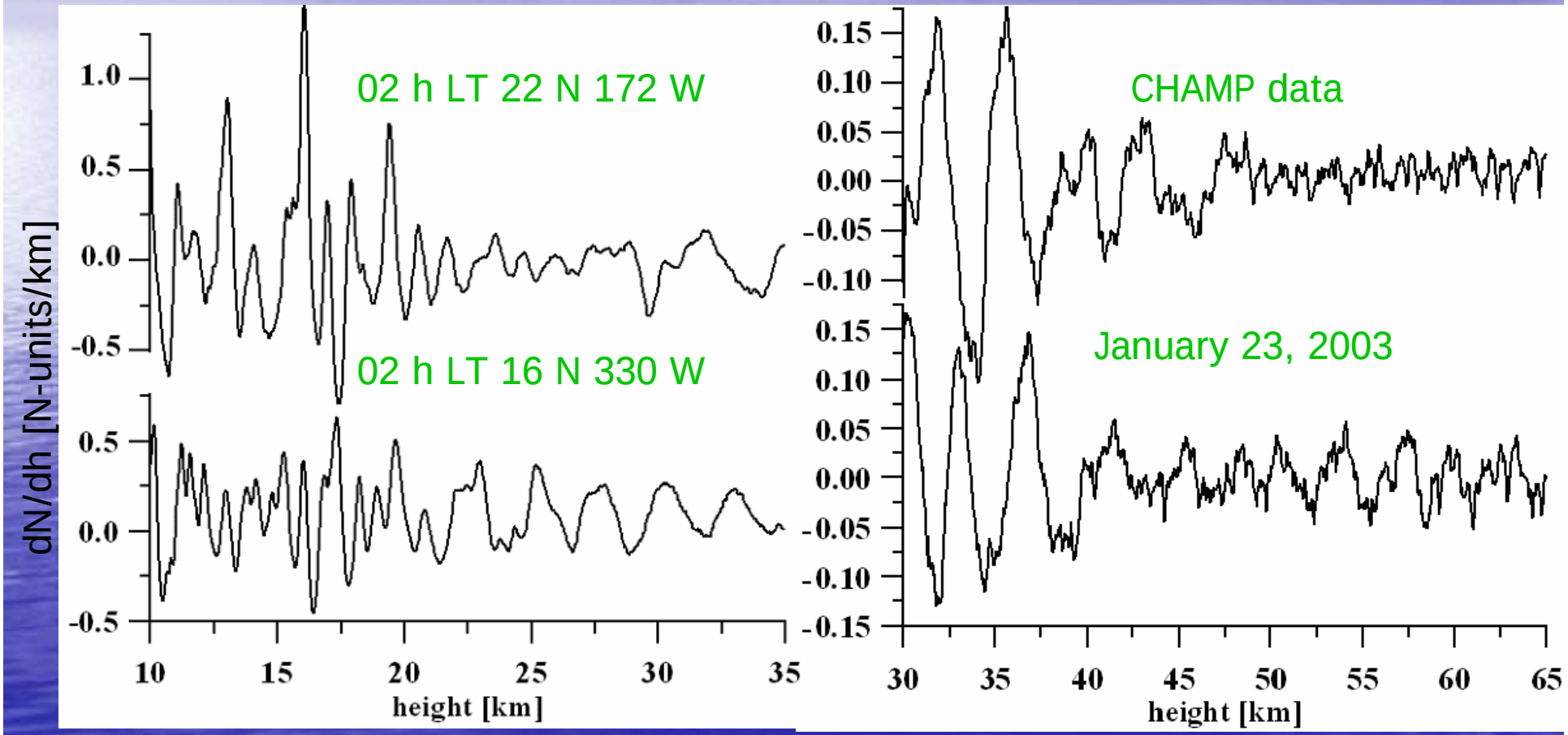

Polarization and dispersion equations for the case when the intrinsic frequency of GW is well below the Brunt-Vaisala frequency ω_b and higher than the inertial frequency f

$$v(h) = \mathrm{Re}[ig/(T_b\omega_b)t(h)],\ \omega_b^2 = g/T_b\Gamma,\ \Gamma = \partial T_b/\partial h + 9.8^0/km$$

$$dv(h)/dh = d\,\mathrm{Re}[ig/(T_b\omega_b)t(h)]/dh \approx \mathrm{Re}[ig/(T_b\omega_b)dt(h)/dh]$$

$$\lambda_h = 2\pi|c - U\cos\varphi|/\omega_b$$

Where

g : gravity acceleration,

T_b: back-ground temperature,

ω_b: Brunt-Vaisala frequency,

U : back-ground wind speed,

C : ground-based horizontal phase speed of the gravity wave

φ: azimuth angle between wind and GW propagation vectors

Note, that the ratio $t(h)/T_b$ can be replaced by $-n(h)/N_b(h)$, where n(h) is the wave perturbations in the refractivity, N_b is back-ground refractivity. Also the factor $(1-f^{**}2/\omega_b{}^{**}2)^{**}-1/2$, must be introduced (Gubenko and Pavelyev, JGR, submitted, 2007)

Left panel: The refraction attenuations *Xa*, *Xp* retrieved from the phase and amplitude data (curve 1 and 2, respectively). Curves 3 indicate the results of simulation of the refraction attenuation in the atmosphere. Right panel: The variations of the vertical gradient of refractivity retrieved from the phase and amplitude data (curve 1 and 2, respectively)

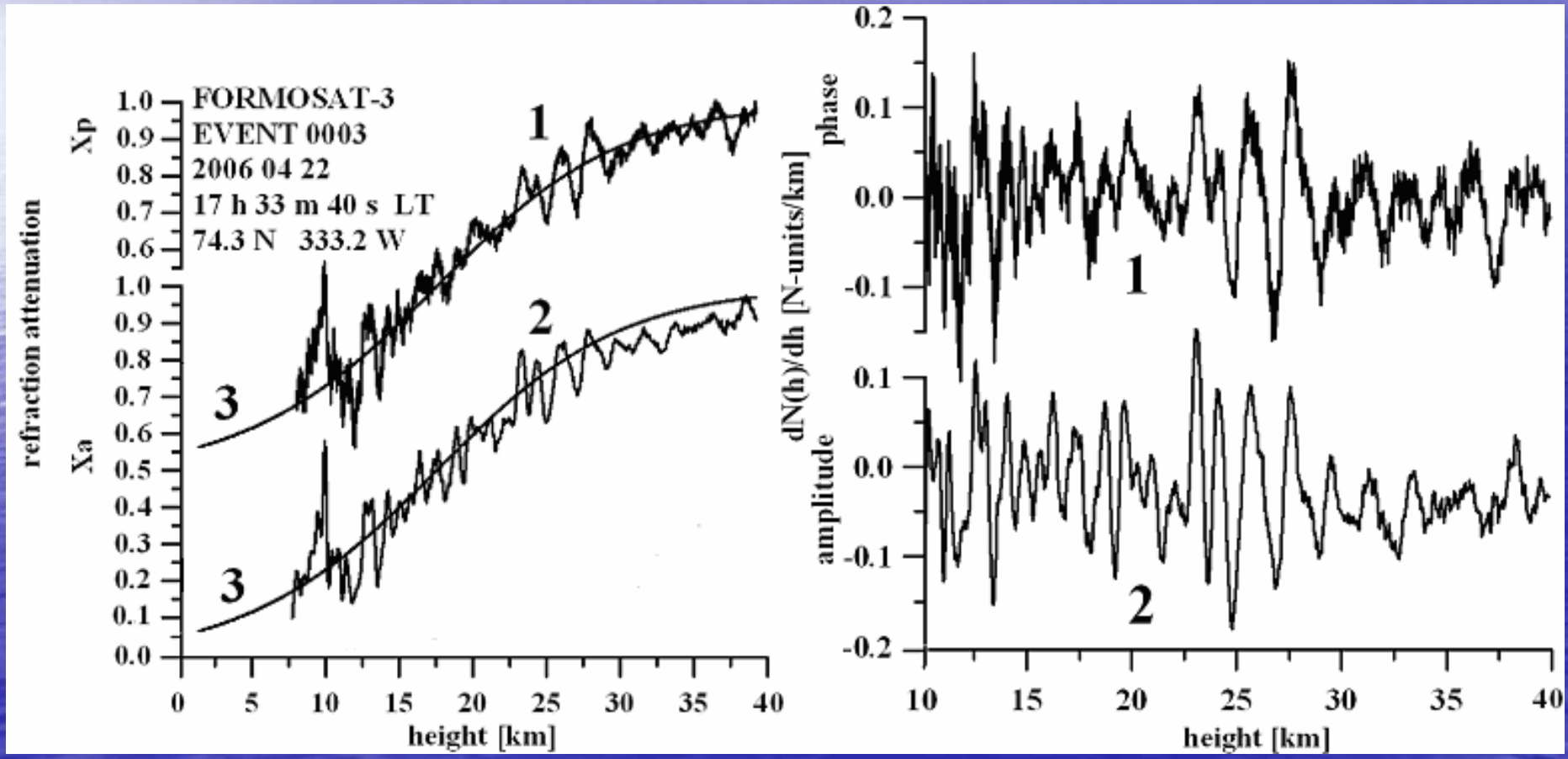

Left panel: vertical profiles of the phase (curves 1 and 2) and amplitude (curves 3 and 4) of GW for CHAMP RO events № 0140 (curves 1 and 3) and № 0001 (curves 2 and 4). Right panel: altitude dependence of the intrinsic phase speed of GW. Curves 1 and 2 correspond to CHAMP RO events № 0140 (02 h 35 m 34 s LT, 21.9 N 172.5 W) and № 0001 (02 h 09 m 51 s LT, 15.9 N 330.0 W), January 23, 2003, respectively

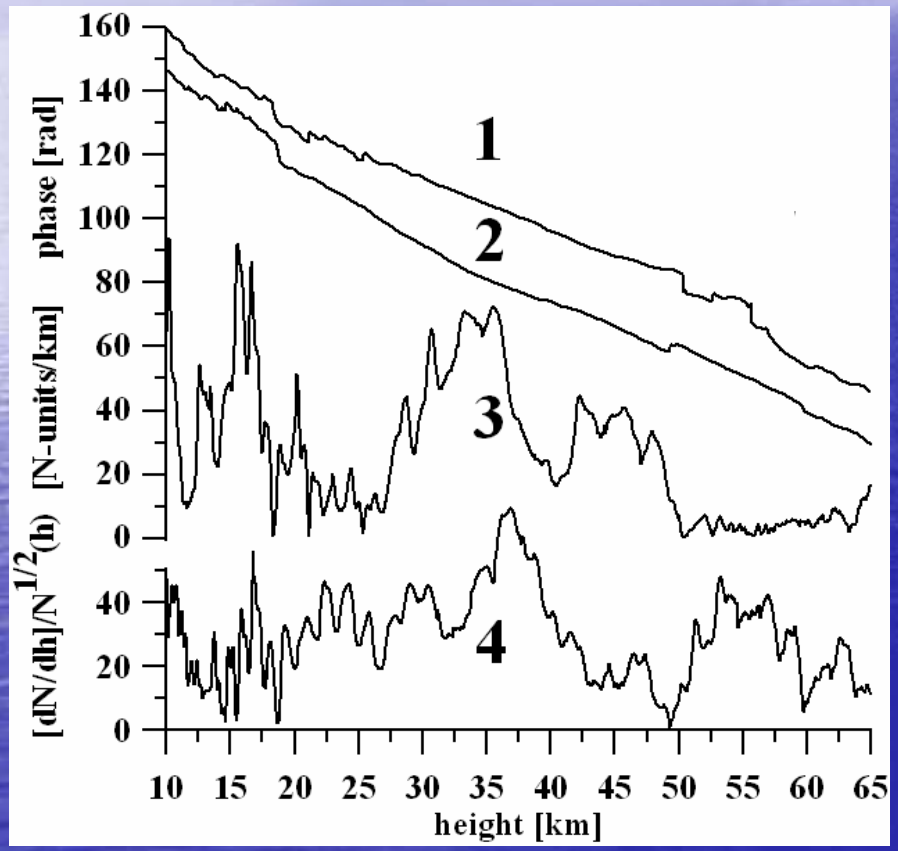

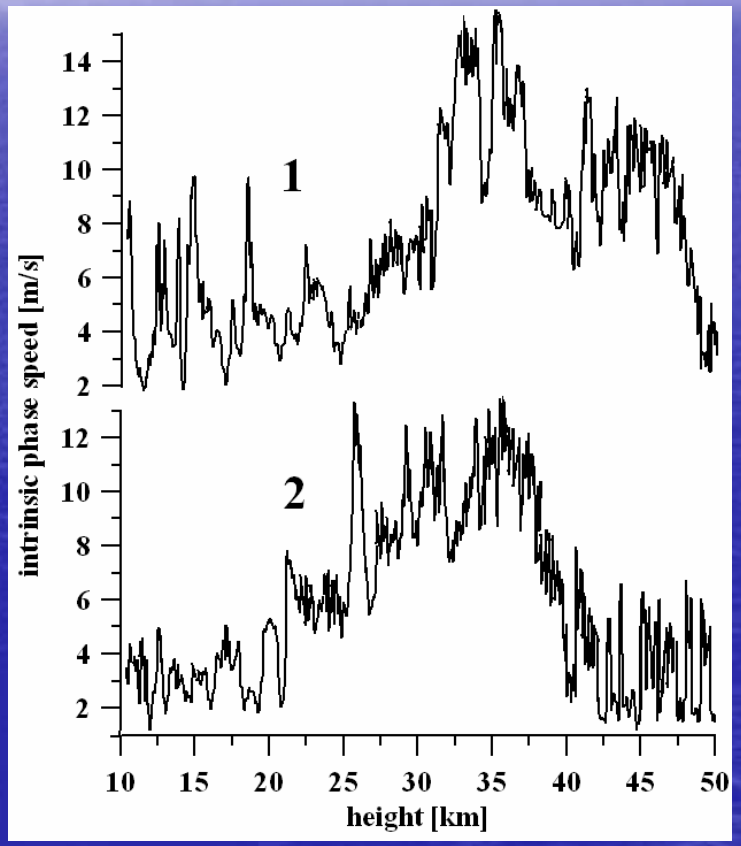

Left panel: The vertical profiles of the horizontal wind perturbations found from the phase and amplitude data (curves 1 and 2, respectively). These variations correspond to the kinetic energy in the internal wave. Right panel: Sum of the kinetic and potential energy of the wave structure.

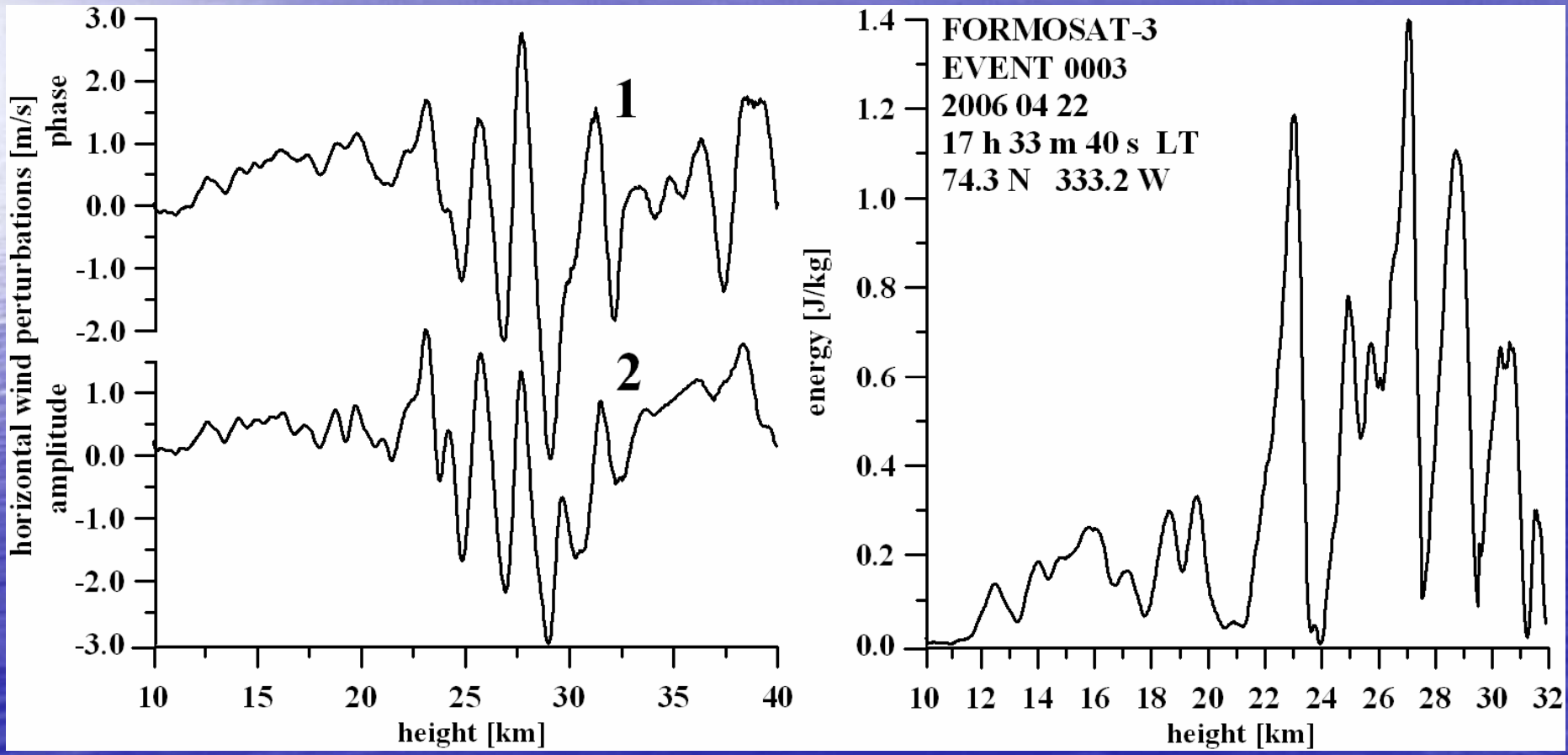

Seasonal and geographical distribution of internal wave activity with amplitudes greater than 1.0 N-units/km (panels 1 and 2, height 12 km) and 0.6 N-units/km (panels 3 and 4, height 14 km) in the lower stratosphere for period November 19 – December 03, 2002 (panels 1 and 3) and June 29 – July 13, 2003 (panels 2 and 4)

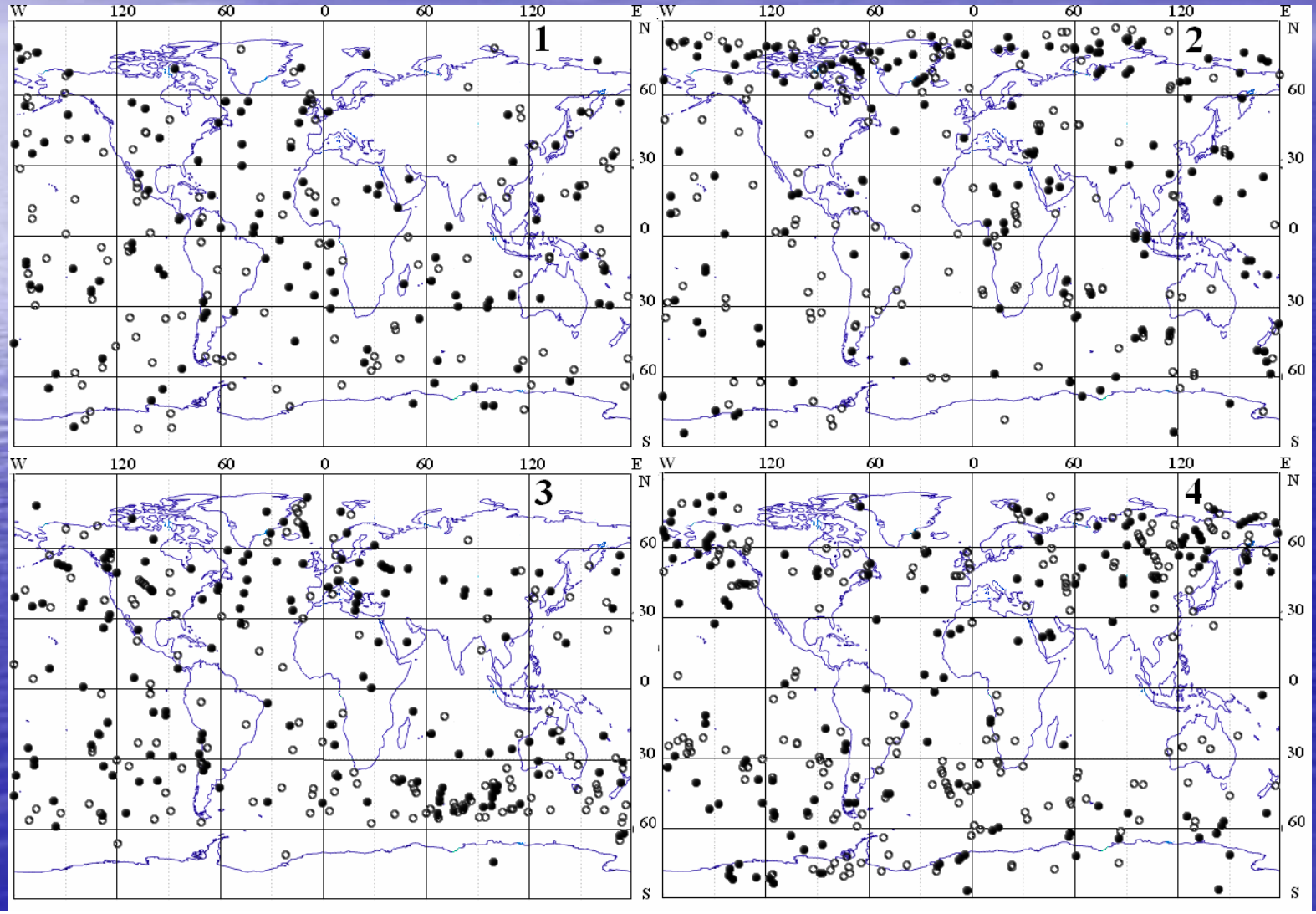

Seasonal and geographical distribution of internal wave activity with amplitudes greater than 0.6 N-units/km in the lower stratosphere for period November 19 – December 03, 2002 (panels 1 and 3) and June 29 – July 13, 2003 (panels 2 and 4). Panels 1 and 2; 3 and 4 correspond to 16 km and 18 km altitude, respectively

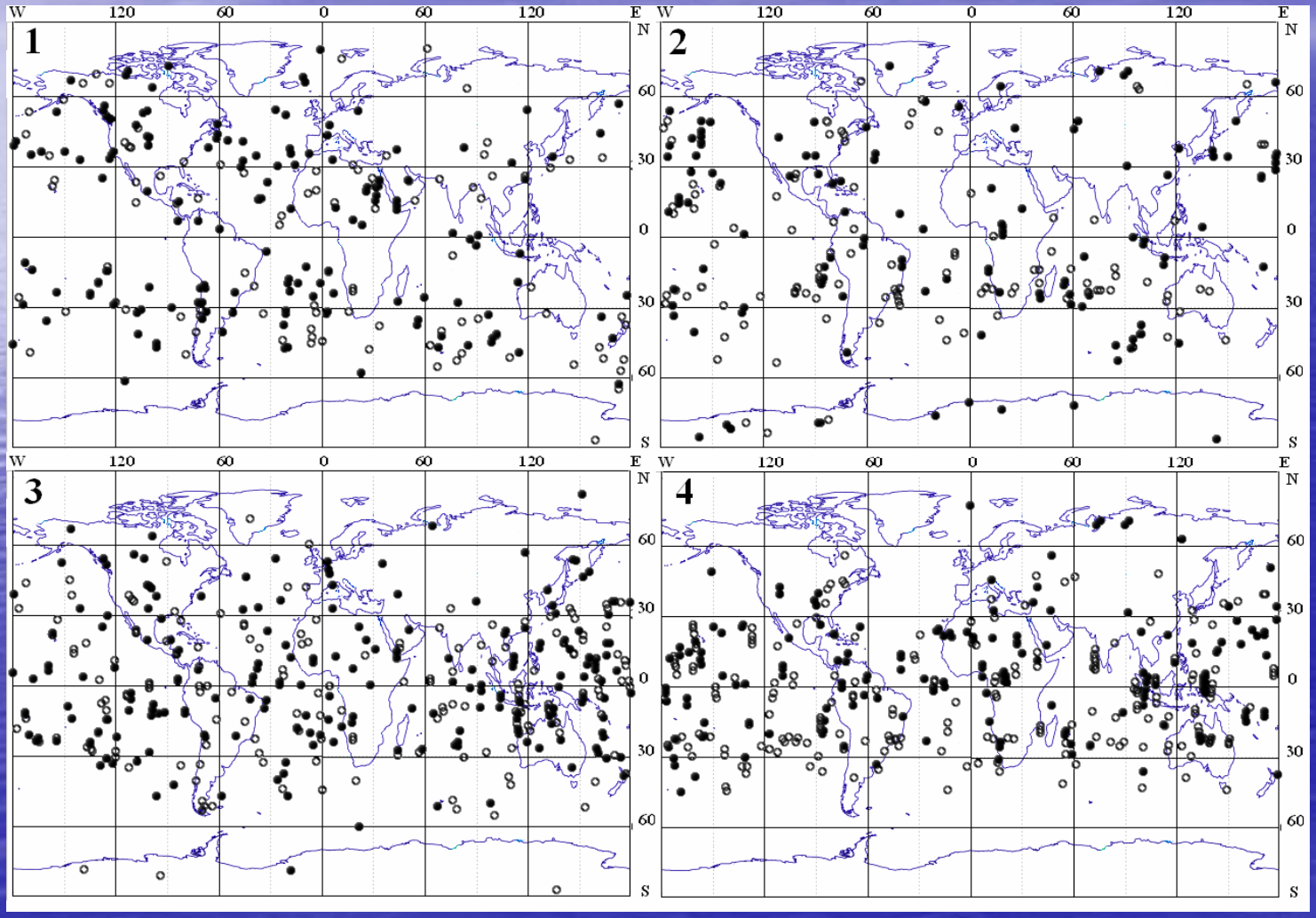

Seasonal and geographical distributions of the wave activity with amplitudes greater than 0.6 N-units/km at the 20 km altitude for periods November 03 – November 18, 2002 (panel 1); December 20, 2002 – January 15, 2003 (panel 2); March 31, 2003 – April 14, 2003 (panel 3); June 29, 2003 – July 13, 2003 (panel 4).

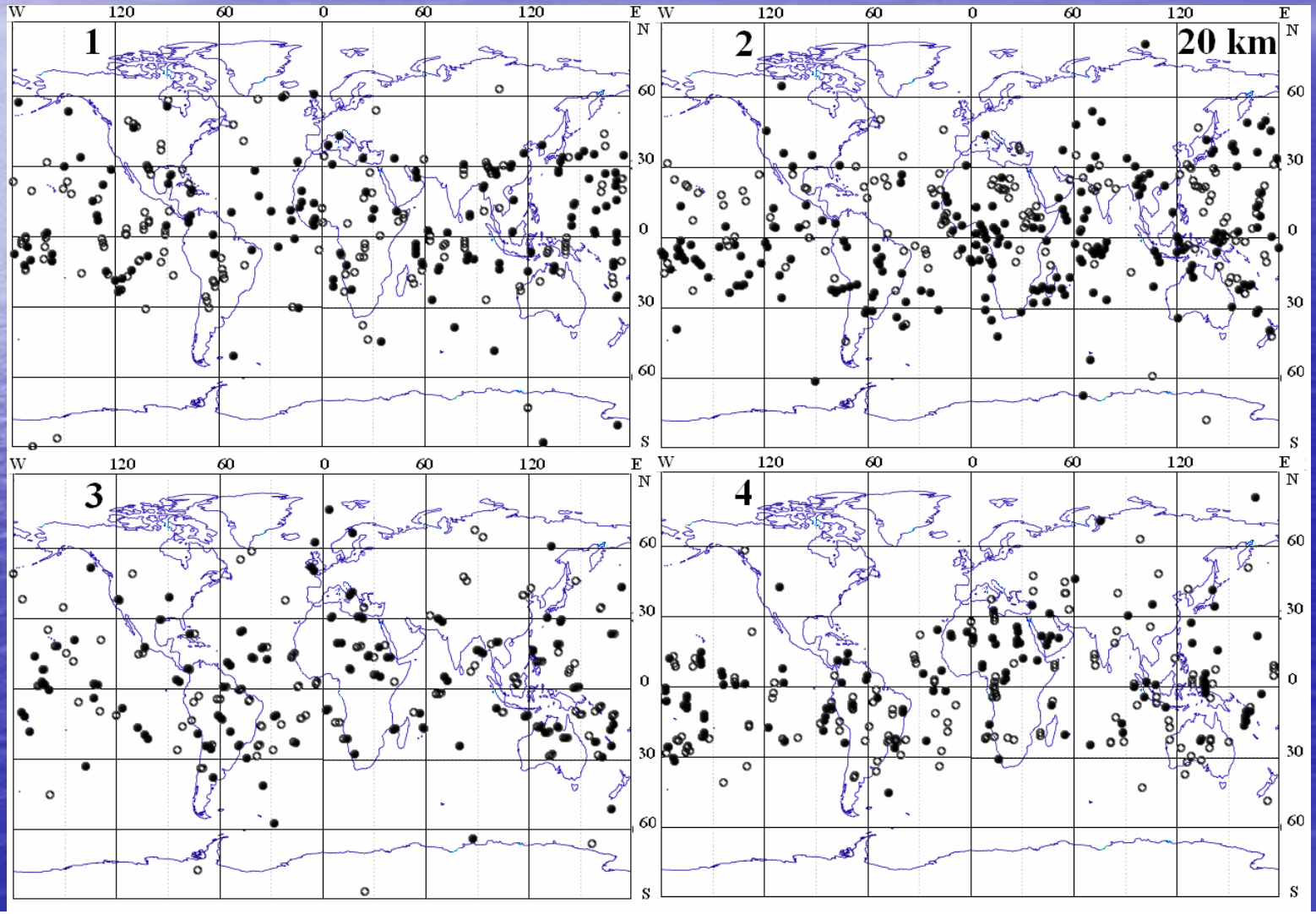

Histograms of wave activity with amplitudes *q* greater than 0.6 N-units/km at the 12 km level for periods July 29 – August 13, 2003 (panel 1); July 13, 2003 – July 27, 2003 (panel 2); March 15, 2003 – March 29, 2003 (panel 3); March 01, 2003 – March 14, 2003 (panel 4). Left: H=12 km. Right: H=14 km.

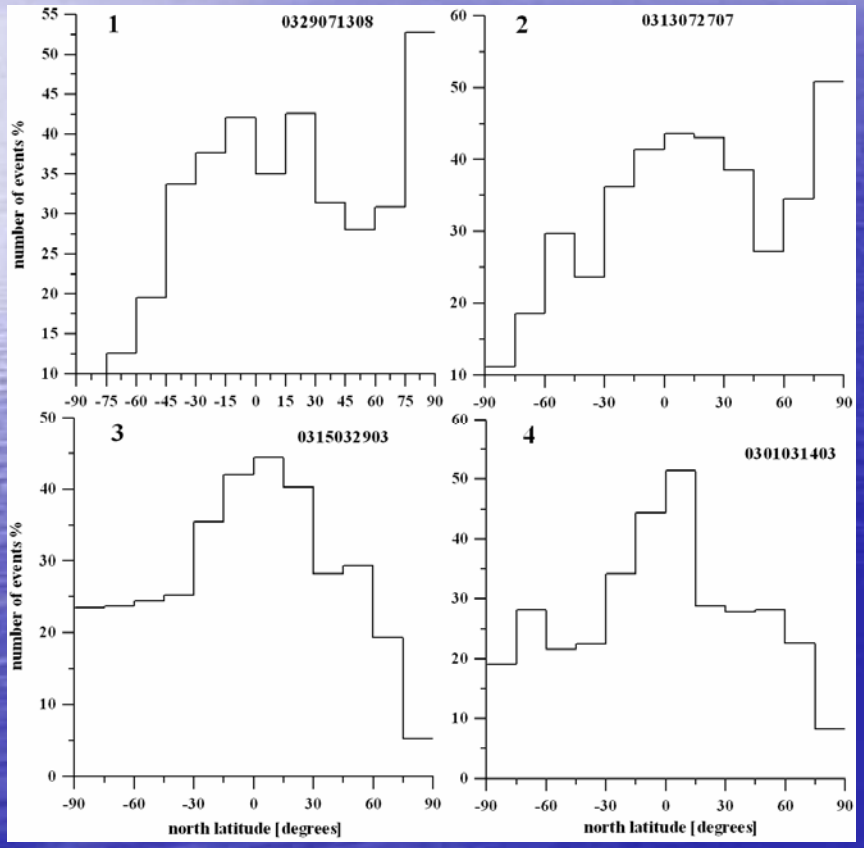

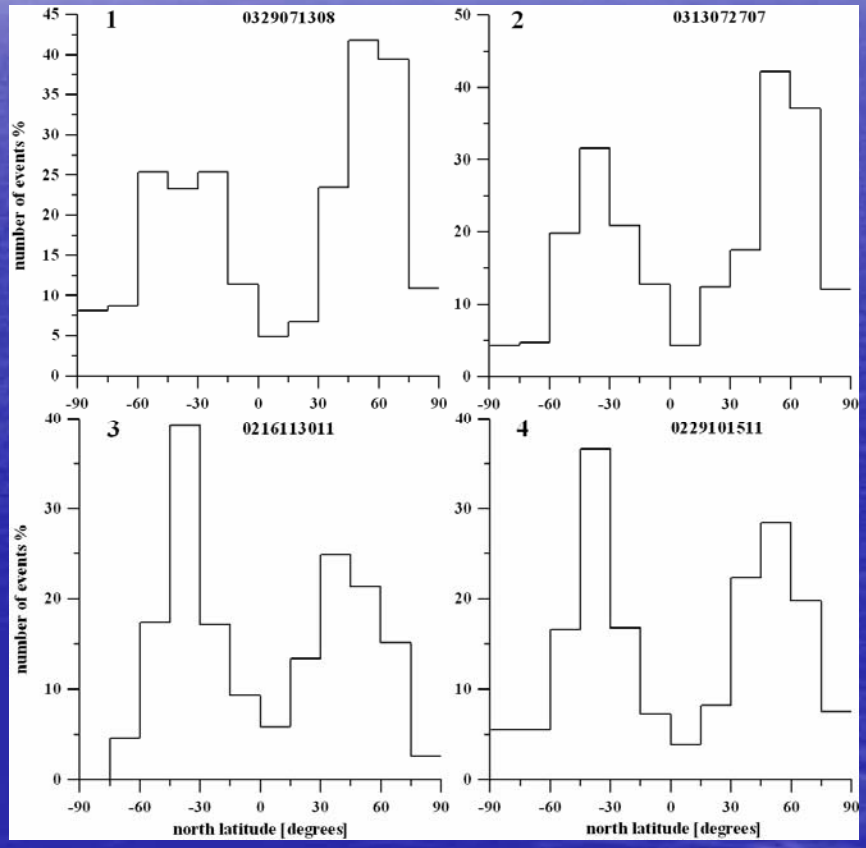

Changes in internal waves activity (averaged over the North (N) and South (S) Hemispheres) during 2001 – 2003 years at different altitudes in the atmosphere. **Right**: 12 km and 14 km (top and bottom panels, respectively). **Left**: 16 and 18 km (top and bottom panels, respectively).

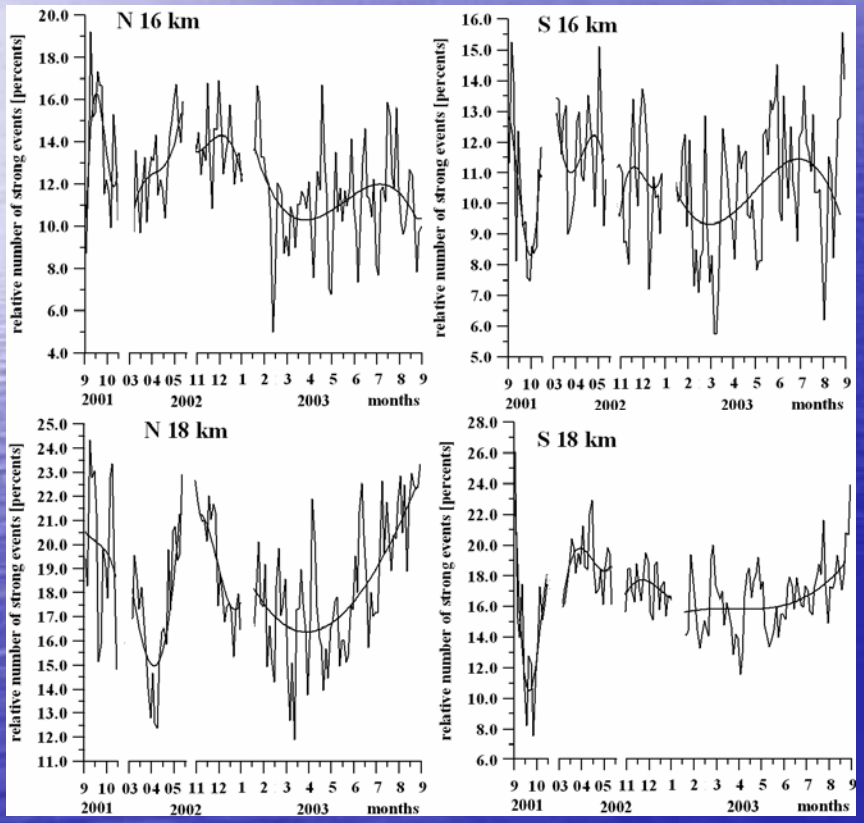

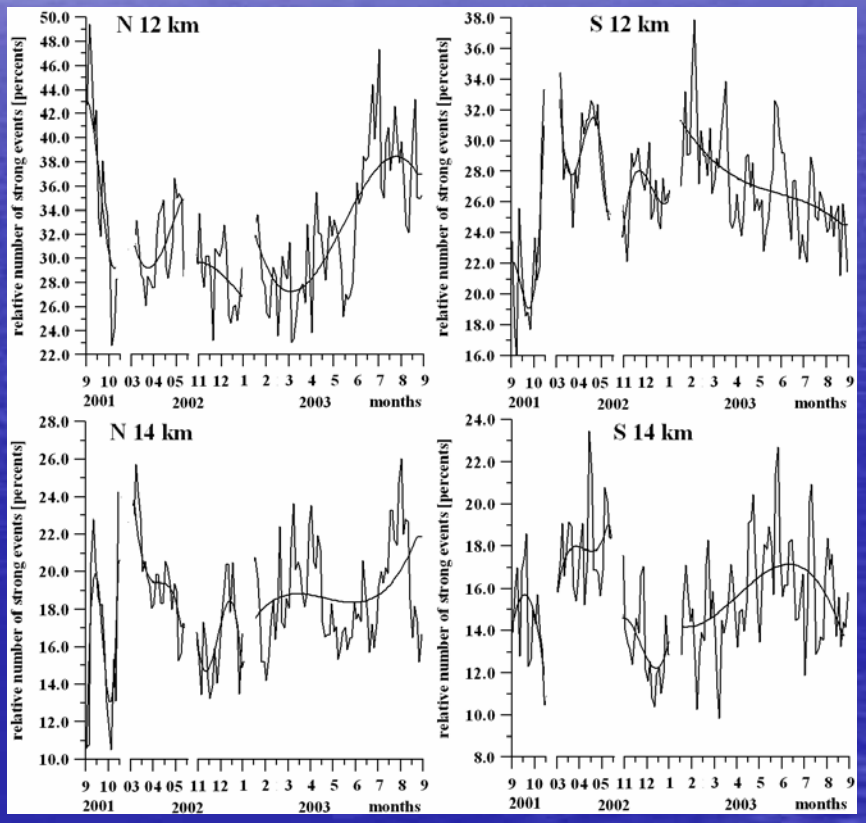

Changes in internal waves activity (averaged over the Earth globe) during 2001 – 2003 years at different altitudes in the atmosphere. **Right**: 20 km and 22 km (top and bottom panels, respectively). **Left**: 24 and 26 km (top and bottom panels, respectively).

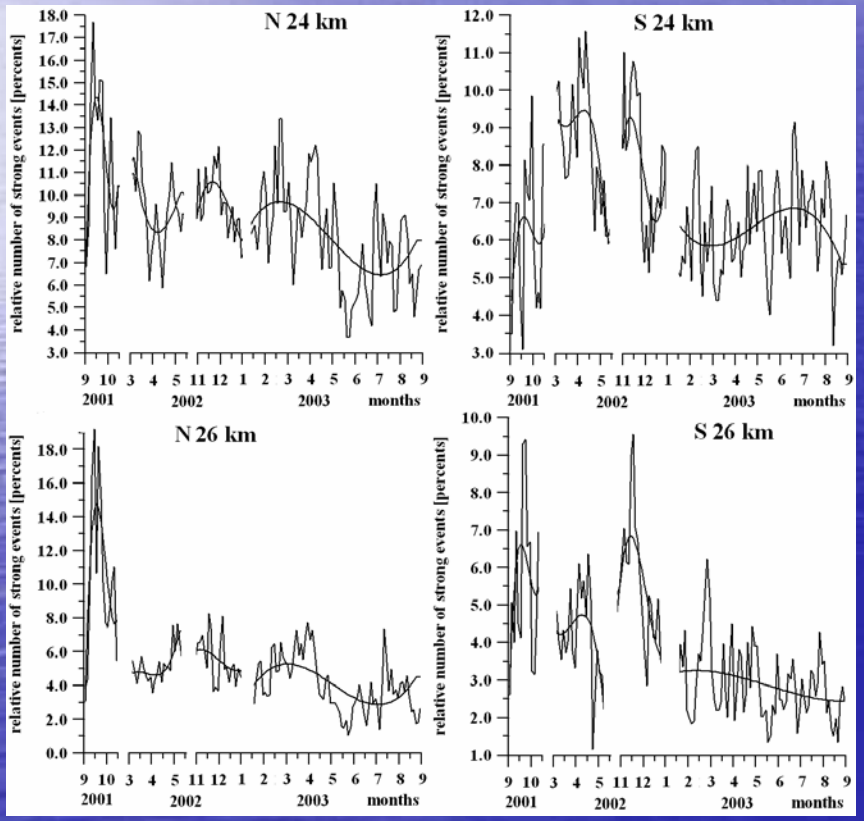

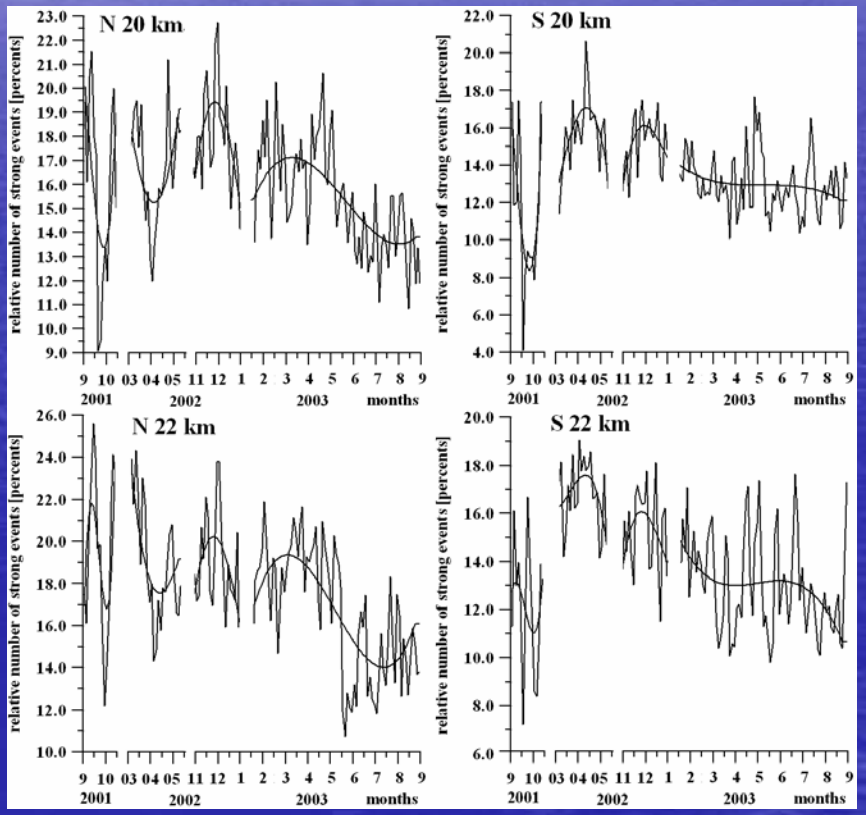

Changes in internal waves activity (averaged over the Earth globe) during 2001 – 2003 years at different altitudes in the atmosphere. **Left**: 20 km and 22 km (top left and right panels, respectively); 24 and 26 km (bottom left and right panels, respectively). **Right**: 12 and 14 km (top left and right panels, respectively); 16 and 18 km (bottom left and right panels, respectively)

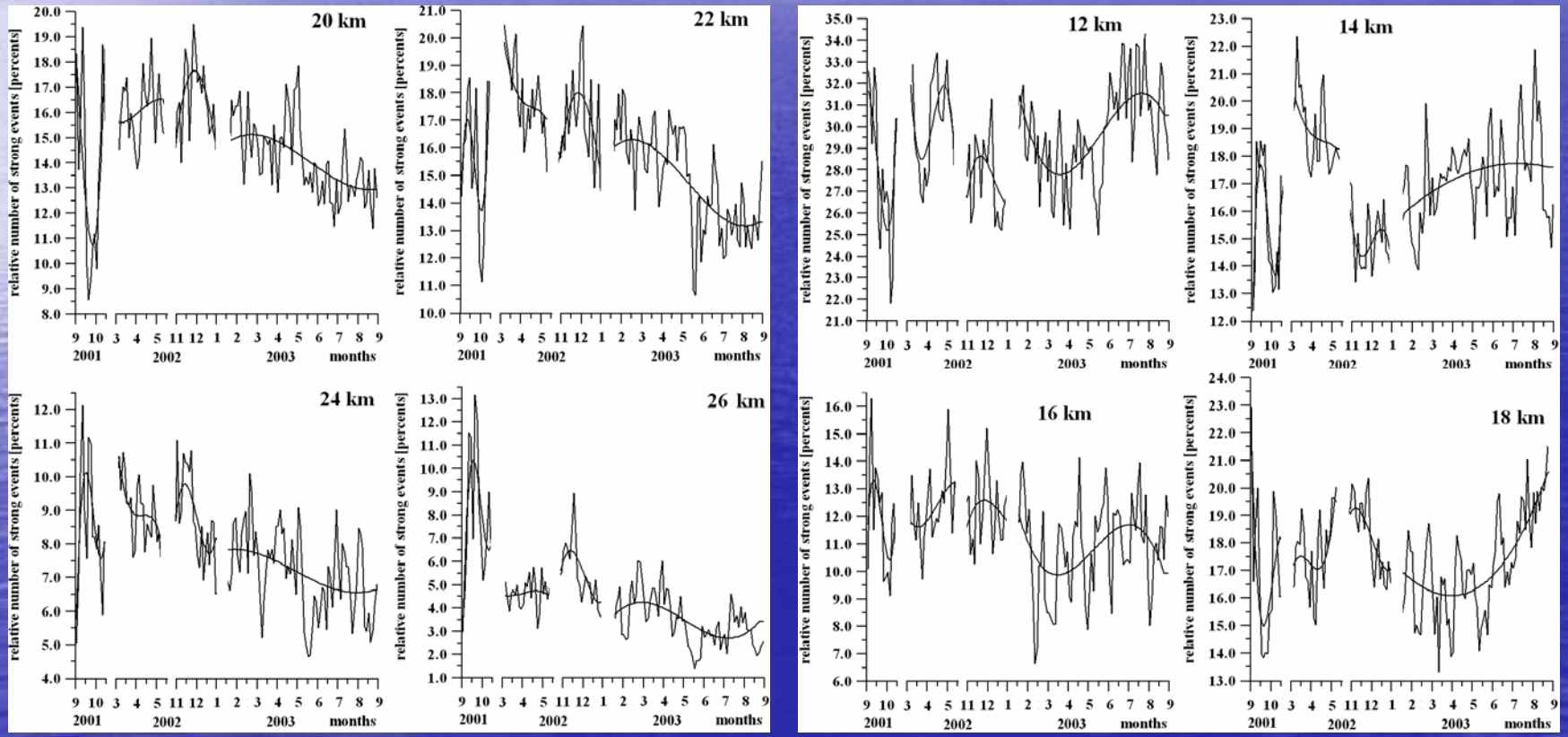

Conclusions

I. The advantages of the introduced relationship consist in

(1) a possibility to separate the layered structure and turbulence contributions to RO signal

(2) a possibility to estimate the absorption in the atmosphere by dividing the refraction attenuations found from amplitude and phase data

(3) a possibility to locate the layered structures in the atmosphere with accuracy in the distance from the standard position of the tangent point of about ±100 km;

(4) a possibility to establish the ionospheric or atmospheric origin of the

amplitude and phase variations of RO signal.

(5) a possibility to estimate horizontal gradients in the lower ionosphere

II. At the first in RO practice the internal wave breaking phenomenon has been observed

III. The internal wave (IW) portrait, which consists of the altitude dependence of the IW phase, amplitude and vertical spatial frequency, can be retrieved from the amplitude and phase variations of the RO signal.

IY. The gravity waves (GW) dispersion and polarization relationships allow one to estimate the vertical profile of the horizontal wind perturbations, its vertical gradient, the GW intrinsic phase speed, the potential and kinetic energy and, under some assumptions, the intrinsic frequency as functions of height in the atmosphere.

Y. At the altitudes 12 km, 16 km, and 20 – 26 km the wave activity is gradually diminishing by 10% – 40% when the time changes from September 2001 to September 2003. This diminishing may be connected with changes in the intensity of the meteorological processes, types of the atmospheric circulations, and, very likely, with reduction in solar activity.

Acknowledgments

We are grateful to NSPO (Taiwan), UCAR (USA) and GFZ-Potsdam (Germany) for access to the GPS/MET, CHAMP, and FORMOSAT-3 RO data. The work has been partly supported by National Science Council of Taiwan (NSC) grant NSC 94-2811-M-008-055 and Russian Foundation for Basic Researches (RFBR) grant No. 06-02-17071.

We are thankful especially to Prof. G. Kirchengast for invitation and fruitful cooperation.

Thank you for your attention!